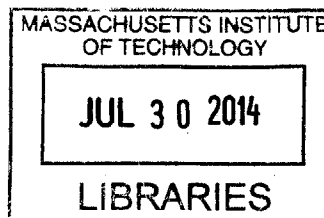


Design of a Triple Singularity Drive for Mobile Wheeled Robots

ARCHIVES

by

Jeffrey Carothers



Submitted to the
Department of Mechanical Engineering
In Partial Fulfillment of the Requirements for the Degree of

Bachelor of Science in Mechanical Engineering

at the

Massachusetts Institute of Technology

June 2014

© 2014 Massachusetts Institute of Technology. All rights reserved.

Signature redacted

Signature of Author:

Department of Mechanical Engineering

May 9, 2014

Signature redacted

Certified By:

V

Harry Asada

Ford Professor of Mechanical Engineering

Thesis Supervisor

Signature redacted

Accepted By:

Anette Hosoi

Professor of Mechanical Engineering

Undergraduate Officer

Design of a Triple Singularity Drive for Mobile Wheeled Robots

by

Jeffrey Carothers

Submitted to the Department of Mechanical Engineering
on May 9, 2014 in Partial Fulfillment of the
Requirements for the Degree of

Bachelor of Science in Mechanical Engineering

ABSTRACT

This thesis encompasses the development of a mobile robotic platform using three singularity drive modules. The process begins with a review of other omnidirectional platforms, comparing and contrasting their strengths and weaknesses. It continues with a discussion of the mechanical and electrical design of a robot prototype, then into kinematic modeling of the system. Both the inverse and forward kinematics are derived and validated through a path following experiment using an open loop controller. For this experiment, the robot was given a 1 meter square path as the desired trajectory, and coded to follow this path at 1 m/s speed. With the open loop controller, the robot was able to track this desired trajectory with a maximum of 16% error in position. An analysis of the results was performed, including discussion on possible sources of error in the system, and areas for future work are explored.

Thesis Supervisor: Harry Asada

Title: Ford Professor of Mechanical Engineering

Acknowledgements

I would like to thank my advisor, Harry Asada, for all of his help in supervising this project, as well as Martin Lozano for all of the assistance he was able to offer me with lab space, materials, and component debugging. Without their dedication and tireless help this project would never have been completed.

I would also like to thank my parents for showing me the importance of hard work and inspiring in me a desire to learn new things. Their support has been monumental in this project and in my life as a whole.

Table of Contents

Abstract	2
Acknowledgements	3
Table of Contents	4
List of Figures	5
List of Tables	6
1. Introduction	7
1.1. Conventional Omnidirectional Drive Systems	7
1.2. Singularity Drive Systems	14
2. Prototype Design	16
2.1. Singularity Drive Module Design	17
2.2. Chassis Design	19
2.3. Electronics System	21
3. Kinematic Modeling	23
3.1. Nomenclature	23
3.2. Inverse Kinematics	25
3.3. Forward Kinematics	31
4. Experimental Model Validation	34
4.1. Experimental Overview	34
4.2. Open Loop Control	34
4.3. Experimental Results	37
4.4. Analysis of Experimental Results	39
5. Summary	41
5.1. Conclusion	41
5.2. Future Work	42
6. Bibliography	43

List of Figures

- Figure 1.** Omni Wheel Design
- Figure 2.** Killough Drive Wheel Layout
- Figure 3.** Four Wheel Omni Drive Configuration
- Figure 4.** Mecanum Wheel Design(a) and Configuration(b)
- Figure 5.** Swerve Drive Wheel Module
- Figure 6.** Ball Drive Module
- Figure 7.** Singularity Drive
- Figure 8.** Singularity Drive Module Overview
- Figure 9.** Chassis Design Features
- Figure 10.** Basic Electrical System Layout
- Figure 11.** Robot Platform Notation
- Figure 12.** Gimbal Angle Notation
- Figure 13.** Position Data for Robot Tracking a 1 Meter Square at 1 m/s
- Figure 14.** Robot Speed During Square Tracking Test

List of Tables

Table 1. Input Signal Versus Motor Drive Speed

Table 2. Drive Motor Control Equations

1. Introduction

1.1 Conventional Omnidirectional Drive Systems

In the field of mobile robotics, a great deal of focus must be placed on methods of locomotion. As technology in the field has advanced, new techniques for mobile robotic platforms have been developed and successfully implemented. Performance parameters such as speed, mobility, and controllability have become more and more important to these systems, and extensive research has been done in recent years to evaluate different drive strategies using these metrics. In almost all circumstances, increasing robot speed, accuracy, and mobility is desired due to the wider range of possibilities for that robot's motion. Most recently, studies have aimed to explore a new branch of robotic locomotion: omnidirectional motion.

Omnidirectional robots are capable of moving in any direction and have full control over their orientation as they move. These robots are often referred to as holonomic, because every possible degree of freedom with which the robot can move on the ground plane can be controlled instantaneously. This is a distinct advantage over traditional drive systems, which suffer from a lack of mobility and often require complex trajectory control in order to arrive at given waypoints. It is much easier for robots to autonomously plan out how and where to move when they are not limited to non-holonomic motion.

There are many different types of omnidirectional drive systems currently in use in mobile robotics. The first method discussed here is known as the three-wheeled Killough drive, or colloquially as the kiwi drive. This system is unique because it uses special wheels,

known as “omni wheels”, which have a series of perpendicular rollers around the circumference of the wheel.

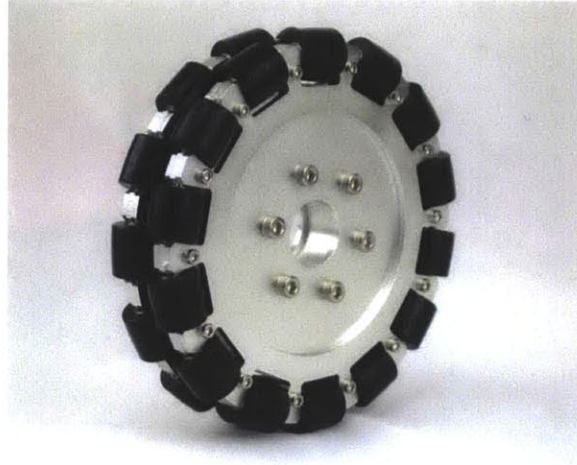


FIGURE 1. OMNI WHEEL DESIGN [Courtesy of Microrobo Inc.]

Figure 1, above, shows the alignment of the rollers to the main drive wheel. This alignment allows the wheel to roll forward and backwards (perpendicular to the main axis of rotation) with full force, yet permits the wheel to roll freely laterally (parallel to the main axis). Thus, these wheels can generate drive forces in one direction while allowing other forces to act on the robot in any other direction. Killough drives exploit this effect by placing three omni wheels on a triangular wheelbase and combining their thrust vectors to produce motion in a desired direction.

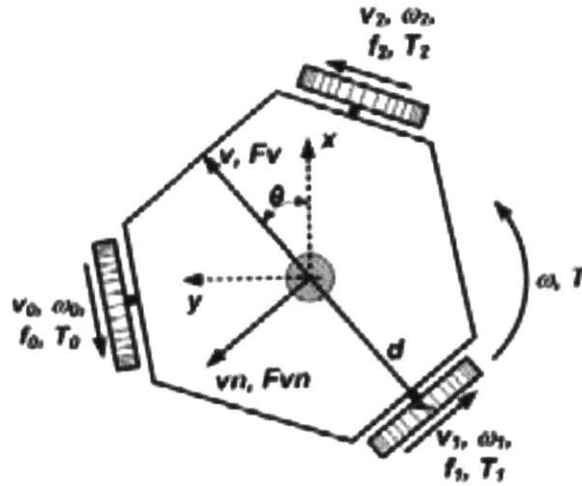


FIGURE 2. KILLOUGH DRIVE WHEEL LAYOUT [3]

Each wheel in a Killough drive produces a drive force, and the three force vectors sum together to produce a net driving force in the desired direction, as depicted in Figure 2 above. It is important to note that each wheel has its own actuator in order to independently control the angular velocity of each wheel. Doing so allows a net thrust vector to be produced in any direction with variable magnitude. Additionally, because the wheels are arranged with their drive axes pointing outward, control over the robot's orientation on the ground plane is possible.

This idea can be implemented with more than just three wheels. Four wheel Killough drives utilize the same force vectoring technique to produce drive forces in any direction, but incorporate an extra wheel for a larger wheelbase and increased drive power. An example of this type of configuration is shown in Figure 3, below.

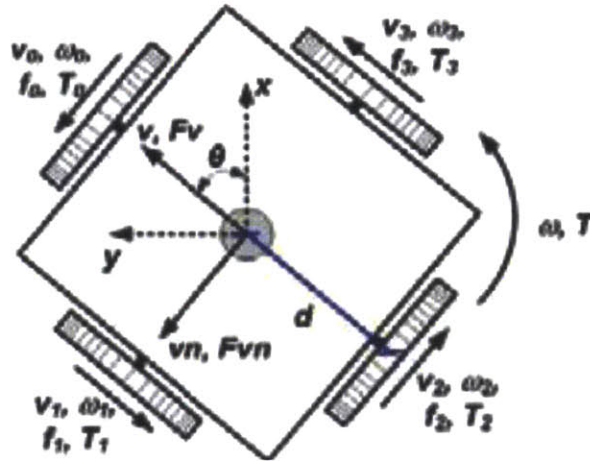


FIGURE 3. FOUR WHEEL OMNI DRIVE CONFIGURATION [3]

Another type of omnidirectional wheeled platform common in ground robots today incorporates a wheel known as the mecanum wheel. Similar to omni wheels, mecanum wheels have a set of rollers along the circumference of the wheel, but instead of being aligned perpendicular to the main drive axis they are aligned at an angle of 45 degrees. This redirects the thrust produced by each wheel in that direction at a decreased magnitude.

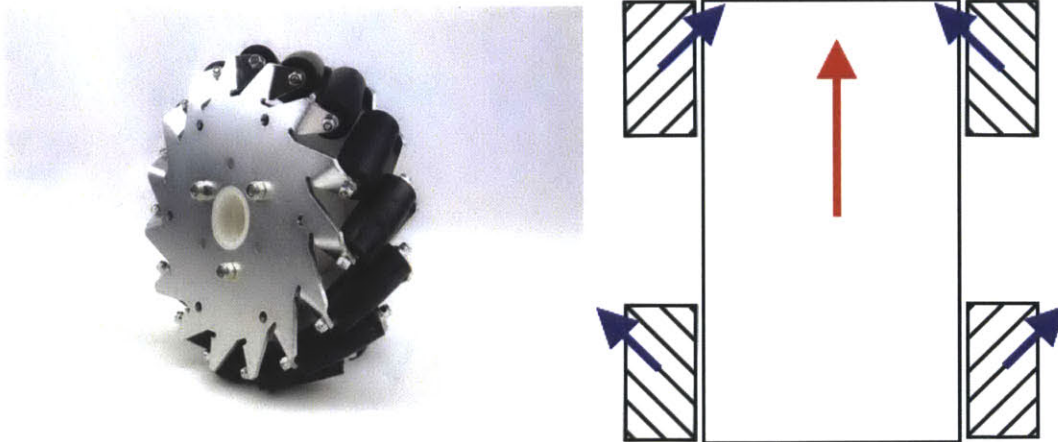


FIGURE 4. MECANUM WHEEL DESIGN(a)

AND CONFIGURATION(b) [Courtesy of Microrobo Inc.]

Figure 4a shows a typical mecanum wheel design and the relationship between drive wheel and the circumferential rollers. Figure 4b shows how these wheels are typically configured on a robot chassis. The angled rollers cause the force vector generated by each wheel to be offset at 45 degrees from the drive axis, which limits the magnitude of force each wheel can create but allows each wheel to contribute a drive force in every cardinal direction. This is useful for many mobile robotic applications where mobility in narrow spaces is critical.

It is important to note that there are a few major drawbacks to roller designs such as the omni and mecanum wheels. By incorporating rollers into the wheel's contact surface, there is inherently slip between the wheel and the ground. This makes localization very difficult and can complicate controller design immensely because it invalidates the no-slip condition assumed in most kinematic models. For omni wheel designs especially, there has been a lot of recent work in developing dynamical models that can account for this slippage, but they are far from perfect [3]. Additionally, omni and mecanum wheel designs suffer from decreased efficiency by nature of the wheels' orientation; each of these designs requires that the thrust vectors produced by each wheel to be oriented in different directions. Because of this, wheels end up pushing against one another in order to generate a net force vector in another direction.

A third type of drive system, known as a swerve drive, can help to minimize these losses. Swerve drives use a set of independently steered wheels to manipulate the chassis. These wheels require two actuators each: one to provide torque to the drive wheel and a second to turn the drive wheel assembly and direct its thrust vector where desired.

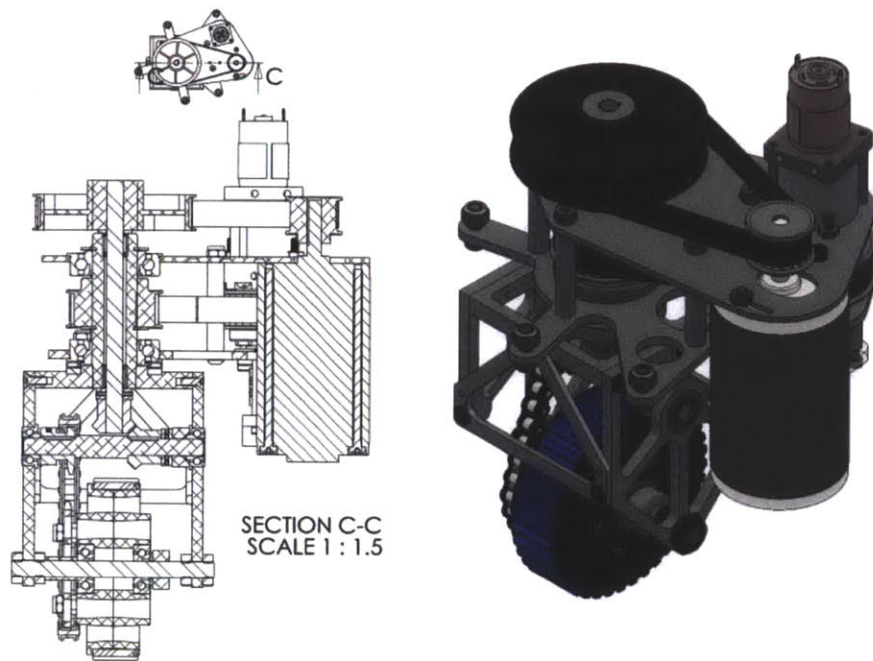


FIGURE 5. SWERVE DRIVE WHEEL MODULE [Courtesy of FRC Team 1640]

Swerve drives are typically built using wheel modules, as shown in Figure 5, which contain both required actuators in a small, modular package. These modules are then arranged as desired on the robot's chassis in either three or four wheel configurations, much like the omni wheel designs discussed above.

Independent control of each wheel's angular velocity and heading allows for control over the robot's movement and orientation. There are no significant power losses in the drive train due to wheels acting against one another, and the lack of rollers maintains complete force transfer from the wheel to the ground. In this way, swerve drives are more efficient than other omnidirectional systems. Nevertheless, having more than two wheels forces the system to be redundant, thereby causing some issues with trajectory tracking. Because each motor is controlled independently, there are always slight discrepancies

between their headings. This causes one or more wheels to slip to accommodate the difference, again creating problems for robot localization and control. Increasing the number of wheel modules can help to reduce this inaccuracy by helping to average out any outlying errors in individual wheels [5]. In truth, swerve drives are not truly omnidirectional, because they are subjected to non-holonomic constraints (ie. the wheel module must turn in place in order to change direction and follow a discontinuous trajectory).

The final common method of omnidirectional locomotion is known as a ball drive. Much as the name implies, this type of system uses spheres in place of traditional wheels to transfer thrust to the ground.

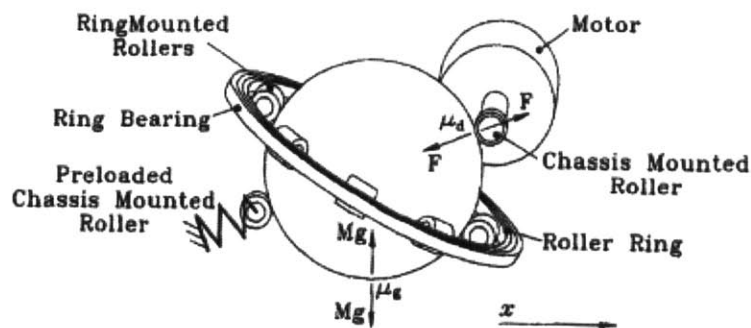


FIGURE 6. BALL DRIVE MODULE [4]

As Figure 6 shows above, ball drives utilize the same modular architecture as swerve drives, but instead of directly driving the ball, independent drive rollers act on it, causing the ball to rotate and direct thrust in the desired direction. This type of drive train is plagued by many of the same problems as other omnidirectional drive systems. First, the

drive rollers must slip on the ball in order to allow the ball to rotate freely. Second, at least three ball modules are required to form a stable ground plane, leading to the same problems of redundancy that plague the swerve drive. These problems combine to make the ball drive very difficult to control accurately.

That said, there are numerous advantages to using a spherical drive system. First, if we assume the driving spheres are hard and the ground is planar, there is only one point of contact between each wheel and the ground. Because of the spherical geometry of the ball itself, this point of contact does not shift with respect to the robot chassis during motion. These combine to create a drive system capable of motion that is instantaneously omnidirectional and extremely smooth [4].

1.2 Singularity Drive Systems

In the last few years, a new type of drive system has seen a surge in interest from the robotics community. This new system, known as a singularity drive, attempts to bring together the benefits of traditional omnidirectional drive systems while reducing their shortcomings.

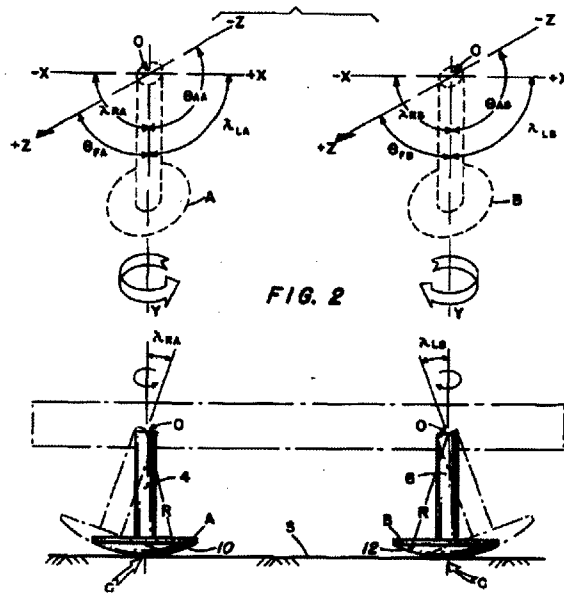


FIGURE 7. SINGULARITY DRIVE [1]

These systems are composed of five main parts: a hemispherical drive wheel, a driving motor, two steering actuators, and a two-axis gimbal. The wheel, which is mounted directly to the gimbal, is powered by the drive motor and has three degrees of freedom as shown in Figure 7. Steering actuators, typically servo motors, manipulate both axes of the gimbal independently. At rest, the hemispherical wheel's axis of rotation is orthogonal to the ground plane. In this neutral position the effective radius of the wheel is zero and no thrust is generated by the wheel's rotation. Steering actuators control the axial and lateral tilt of the wheel via the gimbal, thereby controlling the angle of contact with the ground plane and the effective radius of the wheel. Altering this contact angle can also change which side of the wheel contacts the ground, allowing thrust to be vectored in any direction. Additionally, the magnitude of this tilt determines the effective radius of the wheel at the contact point, which in turn determines the effective gear ratio between the drive motor and ground.

This variable gear ratio allows the singularity drive to direct thrust in any direction with a range of force, without changing the speed or direction of the drive motor. This is very advantageous over the other systems discussed here, because this system can achieve instantaneous omnidirectional movement without the need for closed loop control over the drive motor velocity or position. Even more importantly, there is no minimum requirement for zero-rpm torque, because the singularity drive can maintain an arbitrary speed by adjusting the effective gear ratio of the wheel. Because of this, small, powerful, brushless DC motors can be used for the drive motors, giving the singularity drive a very high power-to-weight ratio as compared to conventional brushed DC motor drivetrains.

As with the other modular systems discussed here, these drive modules can be configured on a robot chassis in different combinations. Research has been done on singularity drive platforms using one and two wheel modules, with passive casters or sliders to stabilize the wheelbase. [5] It is the goal of this thesis to take this research one step further by documenting the design and kinematic validation of a triple singularity drive that utilizes three singularity drive modules for increased stability, power, and trajectory tracking accuracy.

2. Prototype Design

In order to validate this singularity drive system, a prototype robot was designed and a simple trajectory tracking experiment was carried out. The development of this prototype began with the mechanical design. As a proof of concept, the robot was designed and built using rapid prototyping methods such as laser cutting and 3D printing, which allowed new iterations to be implemented quickly and at low cost. The mobile platform can

be broken up into three main component groups: the singularity drive modules, the chassis, and the electronics.

2.1 Singularity Drive Module Design

The most important part of the mechanical design for this robot was the development of the singularity drive modules- without capable drive modules, the robot would be inoperative. These modules include the hemispherical wheel, drive motor, steering actuators, and two-axis gimbal, all of which are combined in a compact, robust, and nimble component.

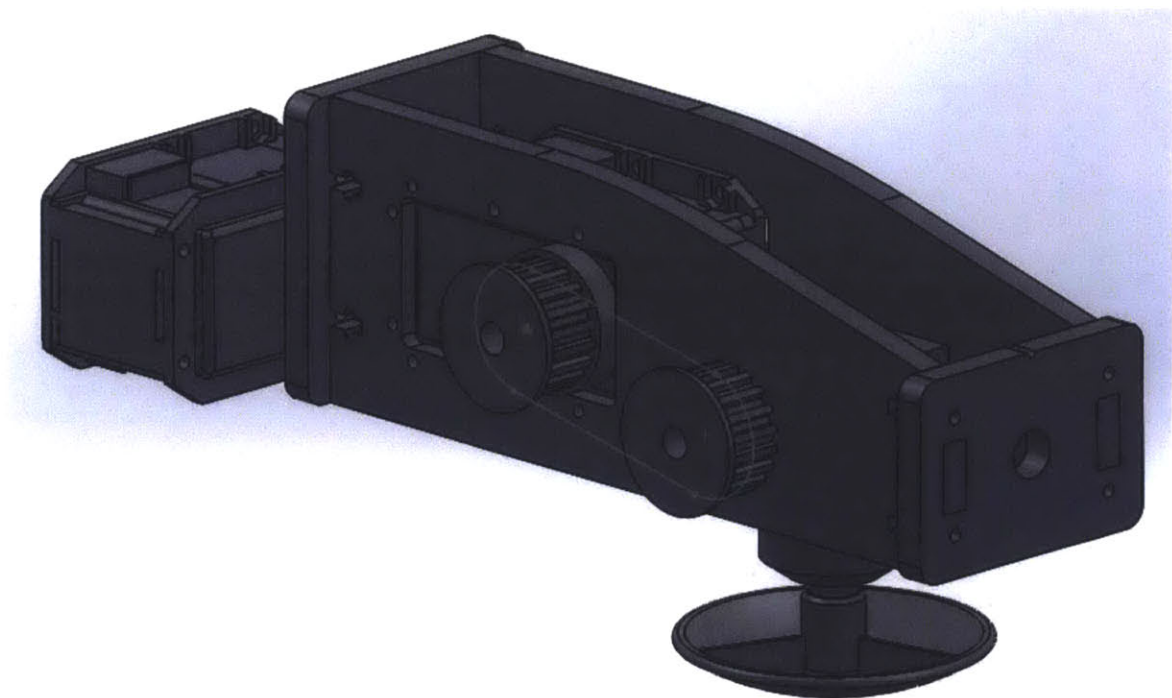


FIGURE 8. SINGULARITY DRIVE MODULE OVERVIEW

Figure 8, above, showcases the design of the drive modules developed for this robot. The most prominent feature is the frame of the module, which is constructed out of

interlocking pieces of acrylic, which were laser cut out of 6mm acrylic. This frame serves as the gimbal body and is able to tilt both axially and laterally as directed by pair of Dynamixel MX-64 Smart Motors. These advanced servo motors are designed for use in robotic applications and have on-board microprocessors and motor drivers that enable them to follow position, velocity, or torque commands using a built-in PID control loop. With approximately 10 W of available power, these motors are the perfect solution for accurately controlling the gimbal angles on this prototype.

Wheel mobility also had to be considered during the design of this prototype, because the drive wheel assembly must be able to tilt freely on the gimbal in order to control the thrust vector that wheel creates. The drive axle must tilt far enough to create a significant effective radius at the wheel, without tilting too far and interfering with the gimbal or chassis. This gimbal assembly was designed to allow the wheel to tilt 30 degrees in any direction (well over the expected maximum expected angle) without interfering with any other components.

Another important consideration for the module design relates to the kinematics of singularity drives. In order to keep the drive's point of contact with the ground at a constant location in the mobile reference frame, the spherical surface of the drive wheel must be centered around the center of the gimbal. Both axes of rotation in the gimbal and the axis of rotation for the drive wheel must all intersect at one point; doing so ensures that the drive maintains instantaneous omnidirectionality and equal mobility in all directions.

Further design effort went into the drive wheel assembly, including the motor and hemispherical wheel. The motors selected to provide driving power were Grayson Foamy

Combo Sport BLDC motors, with a velocity constant of 1100 RPM/Volt. These motors weight only 1.2 oz, yet have over 120 Watts of power capacity- more than enough to propel a robot on this scale. The drive wheel was 3D printed out of ABS, and was designed to be as lightweight as possible, minimizing the wheel's moment of inertia and allowing the drive system to accelerate quickly. Support struts were built into the inner body of the wheel in order to support the contact surface so that the wheel maintained its shape during abrupt direction changes of the robot where high stress is generated.

2.2 Chassis Design

Design of the main robot chassis followed the design of the singularity drive modules and was constructed in much the same way using an interlocking piece of acrylic. As shown in Figure 9, the design is relatively simple, utilizing one large baseplate with attachment points for each of the three singularity drive modules.

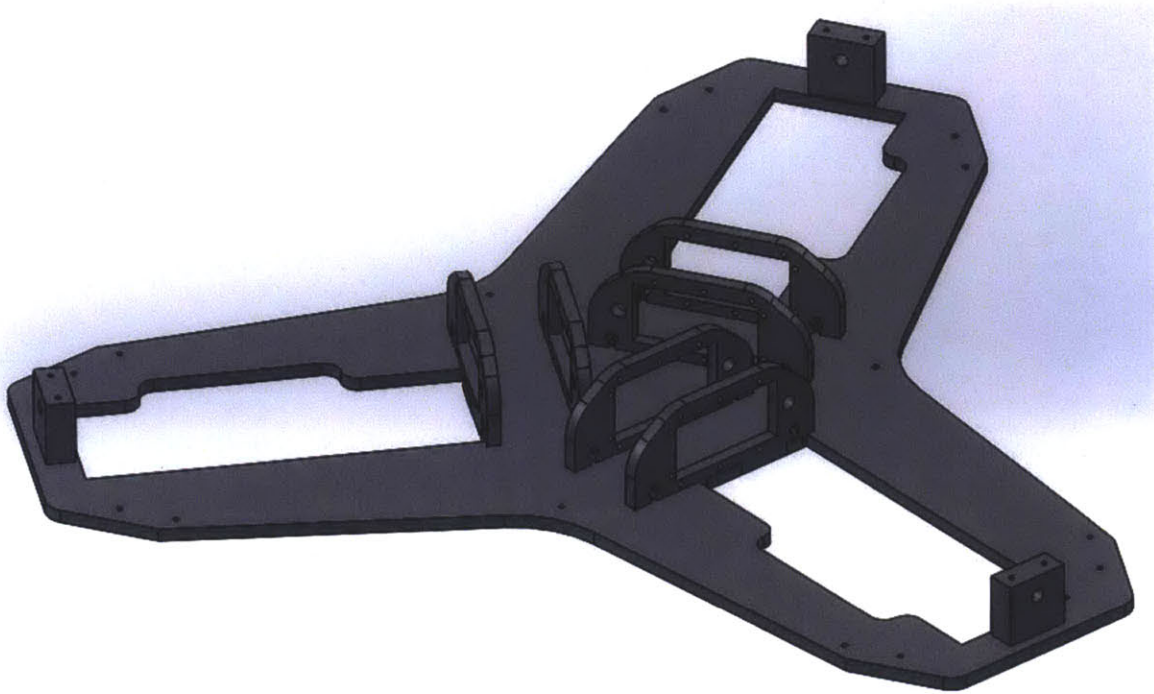


FIGURE 9. CHASSIS DESIGN FEATURES

One of the key features of this chassis design is the modular architecture. Each of the drive modules is held onto the baseplate with a set of screws from the bottom, which allow the modules to be easily removed for repairs, modifications, or updates. Extra mounting features were also included in the design in case future iterations required them. A large concern during the design of this prototype was the structural rigidity of the chassis. It was feared that the weight of the servo motors, drive electronics, and frame may cause bending in the baseplate (thereby throwing the drive modules out of alignment), so extra mounting patterns were cut into the baseplate in case additional bracing needed to be added. After testing the completed robot, however, it was determined that this was unnecessary.

2.3 Electronics System

The control and power electronics used in this prototype were relatively simple. They included an Arduino Mega microcontroller, six Dynamixel servo motors, three brushless motors with their corresponding electronic speed controllers (ESC's), and a remote control radio/receiver pair. The whole system is powered by a 12 volt lead acid battery. A simplified schematic of the system is shown below in Figure 10:

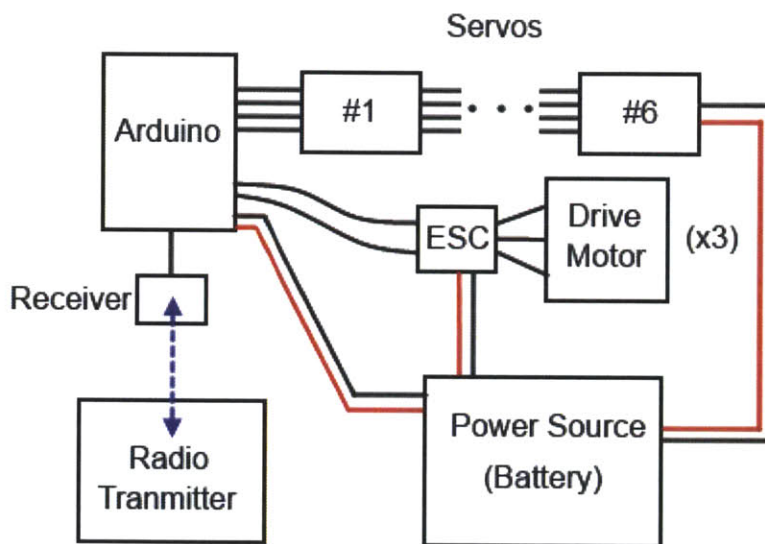


FIGURE 10. BASIC ELECTRICAL SYSTEM LAYOUT

The Arduino Mega was chosen for functionality, cost, and available supporting documentation. With 3 serial connections, the Mega is able to communicate with the chain of Dynamixel servos and a connected computer at the same time, allowing for fine tuning of the singularity drive modules in real time. Additionally, it can communicate through Pulse Width Modulation with the radio receiver and the ESC's using its analog ports. Built-in libraries support both of these communication methods, allowing the Arduino to take

command inputs from remote control, calculate driving parameters, and communicate them to the servos and drive motors very quickly and with minimal computational time. With extensive documentation and an active support network, the Arduino system was ideal for this prototype.

3. Kinematic Modeling

This section of the paper deals with the geometric kinematic modeling of a triple singularity drive mobile platform. This modeling is split into two parts: inverse kinematics, which can be used to solve for the steering angles of the singularity drive modules given a desired robot trajectory, and the forward kinematics, which can be used to estimate the position and orientation of the robot using sensor data.

To solve for these equations, we break the desired motion of the robot into two components: translation of the center of mass and rotation about the center of mass. By superposition, any motion of the robot can be decoupled into these two components. In order to simplify the kinematics, we make the following assumptions:

- There is no slip between the drive wheels and the ground.
- The robot operates on a smooth, hard ground plane.
- The center of mass is perfectly balanced between each of the singularity drive modules, and each point of contact with the ground supports equal weight.
- The motion of the gimbals does not significantly change the location of the center of mass in the mobile reference frame.

3.1 Nomenclature

$O-XY$: the global coordinate system

$O-X_RY_R$: the robot's inertial coordinate system, centered about the center of mass

$O-X_WY_W$:	the singularity drive wheel coordinate system, centered on the pivot point of the singularity drive module
V_x, V_y, ω :	the linear and angular velocity components of the robot in the global reference frame
V_{Rx}, V_{Ry}, ω_R :	the linear and angular velocity components of the robot in the inertial reference frame
V_{Wx}, V_{Wy}, ω_W :	the linear and angular velocity components of the robot in the wheel reference frame
v_w :	the wheel velocity vectors in the inertial reference frame
v_{wx}, v_{wy} :	the components of the wheel velocity vector in the $O-X_RY_R$ coordinate system
v_{wr}, v_{wt} :	the rotational and translational components of the wheel velocity vectors
R :	the distance from the center of mass of the robot to the ground contact point of the singularity drive module
θ_w :	the wheel angle of each singularity drive
ω_d :	the angular velocity of the drive wheels
r_{eff} :	the effective radius of the drive wheel in contact with the ground
γ :	the tilt angle of the drive shaft, measured from the ZW axis
θ_t :	the gimbal steer angle

- α, β : the axial and lateral gimbal rotation angles
- l : the unit vector along the drive axis of the singularity drive
- x_l, y_l, z_l : the components of the unit vector l in the $O-X_W Y_W$ coordinate system
- d_l, h : the projections of unit vector l in the $Z_W X_W$ and $X_W Y_W$ planes respectively

3.2 Inverse Kinematics

We begin the kinematic modeling of the singularity drive with the inverse kinematics. These relationships govern the motion of the robot in response to steering servo inputs and drive wheel angular velocity. Shown in Figure 11 below is the notation used in this derivation.

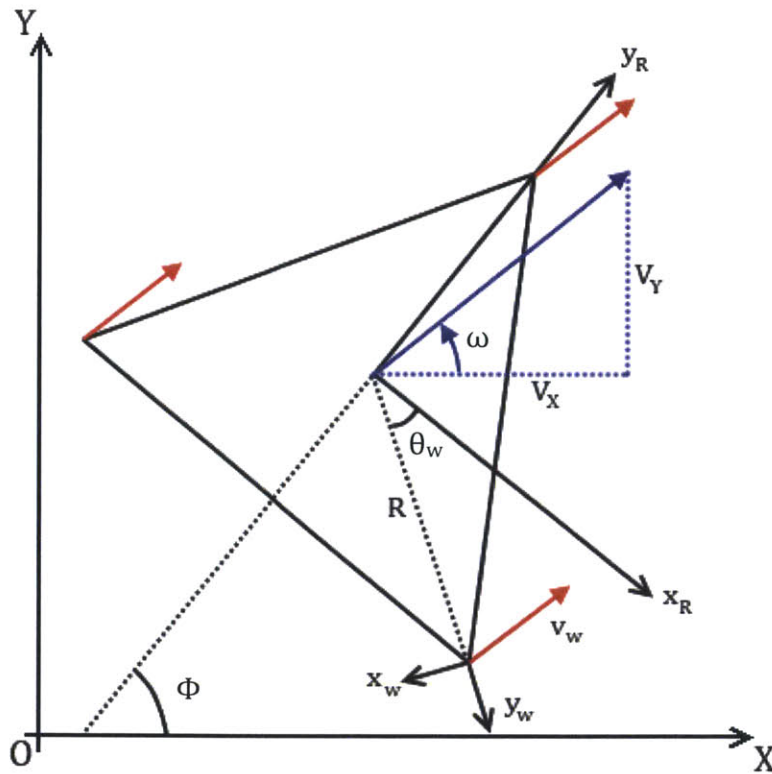


FIGURE 11. ROBOT PLATFORM NOTATION

There are three coordinate systems used in this derivation. First is the world (static) reference frame, labeled $O-XY$; second is the mobile (robot) reference frame, labeled $O-X_RY_R$ and located at the center of mass; and third is the wheel reference frame, labeled $O-X_WY_W$ and fixed to the center point of the gimbal/drive wheel assembly. The angle between the X and X_R axes, which defines the robot's global orientation, is Φ . Input parameters for the inverse kinematics are the desired components of velocity V_X and V_Y and the angular velocity ω of the robot with respect to the static reference frame $O-XY$. In order to express these desired movement vectors in the mobile reference frame, we use the following coordinate transformation:

$$\begin{bmatrix} v_{Rx} \\ v_{Ry} \\ \omega_R \end{bmatrix} = \begin{bmatrix} \cos \phi & \sin \phi & 0 \\ -\sin \phi & \cos \phi & 0 \\ 0 & 0 & 1 \end{bmatrix} \begin{bmatrix} V_X \\ V_Y \\ \omega \end{bmatrix} \quad (1)$$

The motion of the robot is broken down into two components: translational and rotational. Corresponding velocity vectors at each wheel (v_w) can be decoupled into these components as well. The magnitude of these wheel velocity vectors is given by the following equation, where R is the distance from the center of mass to the wheel:

$$|v_{wr}| = \frac{\phi_R}{R} \quad (2)$$

The angle between each wheel and the X_R -axis of the mobile coordinate system is denoted by θ_w . The rotational component of the i -th ($i = 1, 2, 3$) wheel velocity vector is given by:

$$\begin{bmatrix} v_{wrx} \\ v_{wry} \end{bmatrix}_i = \begin{bmatrix} 0 & 0 & \frac{\sin \theta_{wi}}{R} \\ 0 & 0 & \frac{\cos \theta_{wi}}{R} \end{bmatrix} \begin{bmatrix} v_{Rx} \\ v_{Ry} \\ \omega_R \end{bmatrix} \quad (3)$$

The translational component of the i -th wheel velocity vector is equivalent to the desired robot velocity \mathbf{v}_R :

$$\begin{bmatrix} v_{wtx} \\ v_{wty} \end{bmatrix}_i = \begin{bmatrix} 1 & 1 & 0 \\ 1 & 1 & 0 \end{bmatrix} \begin{bmatrix} v_{Rx} \\ v_{Ry} \\ \omega_R \end{bmatrix} \quad (4)$$

By superposition, we can sum Equations 3 and 4 in order to find the expression for the i -th wheel velocity vector:

$$\mathbf{v}_w = \mathbf{v}_{wr} + \mathbf{v}_{wt} \quad (5)$$

$$\begin{bmatrix} v_{wx} \\ v_{wy} \end{bmatrix}_i = \begin{bmatrix} 1 & 1 & \frac{\sin \theta_{wi}}{R} \\ 1 & 1 & \frac{\cos \theta_{wi}}{R} \end{bmatrix} \begin{bmatrix} v_{Rx} \\ v_{Ry} \\ \omega_R \end{bmatrix} \quad (6)$$

Another coordinate transformation will allow these wheel velocity vectors to be expressed in their respective wheel's coordinate system:

$$\begin{bmatrix} v_{wx} \\ v_{wy} \end{bmatrix}_i = \begin{bmatrix} \cos \theta_{wi} & \sin \theta_{wi} \\ -\sin \theta_{wi} & \cos \theta_{wi} \end{bmatrix} \begin{bmatrix} v_{wx} \\ v_{wy} \end{bmatrix} \quad (7)$$

By combining Equations 1, 6, and 7, we can find the full kinematic relationship between the desired global velocity, orientation, and the wheel velocity vectors:

$$\begin{bmatrix} v_{wx} \\ v_{wy} \end{bmatrix}_i = \overline{H}_i \begin{bmatrix} V_x \\ V_y \\ \omega \end{bmatrix} \quad (8)$$

$$\begin{bmatrix} v_{wx} \\ v_{wy} \end{bmatrix}_i = \begin{bmatrix} H_{11} & H_{12} & H_{13} \\ H_{21} & H_{22} & H_{23} \end{bmatrix} \begin{bmatrix} V_x \\ V_y \\ \omega \end{bmatrix} \quad (9)$$

Where:

$$H_{11} = \cos \phi (\cos \theta_{wi} + \sin \theta_{wi}) - \sin \phi (\cos \theta_{wi} + \sin \theta_{wi})$$

$$H_{12} = \cos \phi (\cos \theta_{wi} + \sin \theta_{wi}) + \sin \phi (\cos \theta_{wi} + \sin \theta_{wi})$$

$$H_{13} = \frac{2 \cos \theta_{wi} \sin \theta_{wi}}{R}$$

$$H_{21} = \cos \phi (\cos \theta_{wi} - \sin \theta_{wi}) - \sin \phi (\cos \theta_{wi} - \sin \theta_{wi})$$

$$H_{22} = \cos \phi (\cos \theta_{wi} - \sin \theta_{wi}) + \sin \phi (\cos \theta_{wi} - \sin \theta_{wi})$$

$$H_{23} = \frac{\cos^2 \theta_{wi} - \sin^2 \theta_{wi}}{R}$$

The magnitude of the wheel velocity is equal to:

$$|v_W| = \sqrt{v_{Wx}^2 + v_{Wy}^2} \quad (10)$$

Equation 9 dictates the wheel velocity vectors with respect to each wheel's own reference frame. Next, we need to determine the gimbal angles that correspond to these desired wheel velocities. First, we consider the tilt angle of the drive wheel assembly. Recall that this angle directly determines the effective gear ratio of the drive assembly by altering the effective radius of the wheel. The necessary effective radius to match the desired speed is given by the following equation, where ω_d is the angular velocity of the drive motor:

$$r_{eff} = \frac{|v_W|}{\omega_d} \quad (11)$$

In this case, because there is an infinitely variable gear ratio between the drive motor and the ground, the motor speed is held constant and can be an arbitrary value. The

relationship between gimbal tilt angle γ and the effective radius of the drive wheel is given here, where r_w is the spherical radius of the drive wheel:

$$\sin \gamma = \frac{r_{eff}}{r_w} \quad (12)$$

Combining Equations 11 and 12 gives us an expression for the required tilt angle as a function of drive wheel radius and the desired wheel velocity:

$$\gamma = \sin^{-1} \left(\frac{|v_w|}{\omega_d \cdot r_w} \right) \quad (13)$$

In order to determine the steering angles for the singularity drive gimbals, we need to establish additional notation. Each Y_w -axis is aligned radially outward with the center of the mass of the robot. Let these Y_w -axes correspond to lateral gimbal rotation, while the X_w -axes correspond to axial gimbal rotation; β and α measure the angles of rotation in these respective axes.

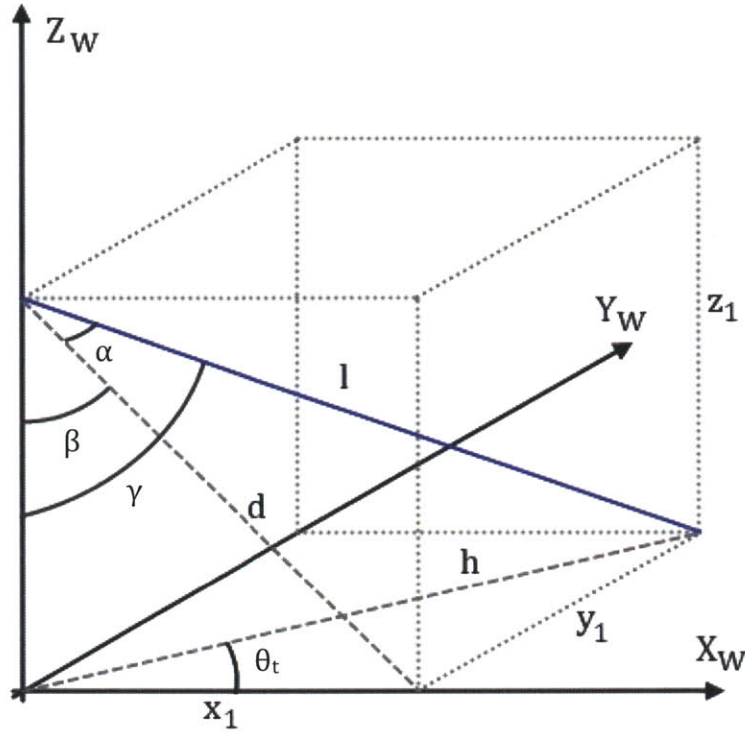


FIGURE 12. GIMBAL ANGLE NOTATION

Let unit vector \mathbf{l} represent the direction of the drive axle in 3D space. Additionally, let x_1 , y_1 , and z_1 represent the three components of unit vector \mathbf{l} in the $O\text{-}X_wY_wZ_w$ coordinate system. Tilt angle γ is measured between vector \mathbf{l} and the Z_w -axis, while the steer angle θ_t measures the angle between the X_w -axis and the projection of \mathbf{l} on the X_wY_x plane (itself denoted as length h). Note that θ_t is perpendicular to the wheel velocity vector v_w due to the spin of the motor shaft (which is positive in the counter clockwise direction from the top):

$$\theta_t = \angle \overrightarrow{v_w} + \frac{\pi}{2} \quad (14)$$

Length d measures the length of vector \mathbf{l} 's projection onto the Z_wX_w plane. The values of z_1 and h are equal to the following:

$$z_1 = l \cos \gamma \quad (15)$$

$$h = l \sin \gamma \quad (16)$$

The lengths of components x_1 and y_1 are equal to:

$$x_1 = l \sin \gamma \cos \theta_t \quad (17)$$

$$y_1 = l \sin \gamma \sin \theta_t \quad (18)$$

Similarly, the length of d is found to be:

$$d = \sqrt{l \cos \gamma + l^2 \sin^2 \gamma \cos^2 \theta_t} \quad (19)$$

Using these values, the values of gimbal angles α and β can be found:

$$\beta = \sin^{-1} \left(\frac{x_1}{d_1} \right) \quad (20)$$

$$\beta = \sin^{-1} \left(\frac{\sin \gamma \cos \theta_t}{\sqrt{\cos \gamma + \sin^2 \gamma \cos^2 \theta_t}} \right) \quad (21)$$

$$\alpha = \sin^{-1} \left(\frac{y_1}{l} \right) \quad (22)$$

$$\alpha = \sin^{-1} (\sin \gamma \sin \theta_t) \quad (23)$$

3.3 Forward Kinematics

The forward kinematics of this system can be used to estimate the global velocity of the robot using angle measurements at each of the singularity drive gimbals. Inputs for the forward kinematics are the gimbal angles α and β . In order to derive the proper relationships, we begin with the same gimbal vector diagram shown in Figure 12. We can solve for x_1 , y_1 , d_1 , and h in terms of the gimbal angles:

$$x_1 = \cos \alpha \sin \beta \quad (24)$$

$$y_1 = \sin \alpha \quad (25)$$

$$h = \sqrt{x_1^2 + y_1^2} \quad (26)$$

We can use these values to solve for the tilt angle γ and the steer angle θ_t :

$$\gamma = \sin^{-1} h \quad (27)$$

$$\theta_t = \tan^{-1} \left(\frac{y_1}{x_1} \right) \quad (28)$$

By combining Equations 12 and 27, we can calculate the effective radius of the drive wheel on the ground:

$$r_{eff} = h \cdot r_w \quad (29)$$

We can rearrange Equation 11 to get an expression for the magnitude of the wheel velocity vector using this effective radius and the angular speed of the drive wheel:

$$|v_w| = w_d \cdot r_{eff} \quad (30)$$

Using this magnitude, Equation 29, and some basic trigonometry, we can find the following expressions for the components of the wheel velocity vectors at each wheel:

$$v_{wxi} = |v_w| \cos \left(\theta_t - \frac{\pi}{2} \right) \quad (31)$$

$$v_{wyi} = |v_w| \sin \left(\theta_t - \frac{\pi}{2} \right) \quad (32)$$

In a traditional system, we could rearrange the inverse kinematic equations and solve for the robot's global velocity and orientation. However, the singularity drive system

is overdetermined, which means that we cannot invert the (non-square) H matrix in Equation 9 to do so. Therefore, we rely on a best-fit solution to find the most accurate approximation of the robot's velocity and orientation.

The following equation takes all of the gimbal angle measurements for three singularity drive modules and produces the most consistent linear and angular velocities of the robot with those measurements- even if those measurements do not agree [2]:

$$\begin{bmatrix} V_X \\ V_Y \\ \omega \end{bmatrix} = \left[\bar{H}_s^T + \bar{H}_s \right]^{-1} \bar{H}_s^T \begin{bmatrix} v_{wx1} \\ v_{wy1} \\ v_{wx2} \\ v_{wy2} \\ v_{wx3} \\ v_{wy3} \end{bmatrix} \quad (33)$$

Where:

$$\bar{H}_s = \begin{bmatrix} \bar{H}_1 \\ \bar{H}_2 \\ \bar{H}_3 \end{bmatrix} \quad (34)$$

4. Experimental Model Validation

4.1 Experiment Overview

This chapter documents the experimental validation of the kinematic model derived in the previous chapter. This validation was performed by implementing a simple open loop controller and commanding the robot to follow a basic square-shaped trajectory. A fixed overhead camera recorded the robot's motion, and image analysis was completed to analyze the position of the robot in each video frame with respect to the global coordinate system. Velocity data was extrapolated from the position data and compared to the reference trajectory.

4.2 Open Loop Control

For the purposes of this thesis, open loop control of the robot was chosen as an ideal proof-of-concept control strategy for the triple singularity drive platform. While closed loop control would enable more precise tracking of a given trajectory, such intensive controller design was beyond the scope of this project.

This open loop controller uses the inverse kinematic equations derived in the previous chapter to cause desired movement in the robot. With a known desired trajectory, Equations X and X can be used to calculate the gimbal angles to produce the appropriate thrust vectors that will drive the robot along the desired path. Before this can be implemented, however, we need to establish a working relationship between the angular velocity of the drive motors and their control signals coming from the Arduino. This will

enable us to accurately establish the angular velocity ω_d , used in the kinematic equations above.

To this end, measurements of the drive wheel's angular velocities were taken using a handheld tachometer for varying input control signals. The results of these tests for each motor are compiled into Table 1, below.

TABLE 1. INPUT SIGNAL VERSUS DRIVE MOTOR SPEED

Input Signal	Angular Speed (rpm)		
	Motor 1	Motor 2	Motor 3
0	0	0	0
20	0	0	0
40	2892	2938	2856
60	4137	4762	4322
80	5895	5768	6147
100	7264	7019	7121
120	8419	9016	8804
140	10113	10205	10353
160	11927	11898	11785
180	13603	13445	13409

As Table 1 shows, even though the drive motors are functionally identical, they do not spin at exactly the same speed when given the same control signal. While the kinematic equations can take this into consideration and maintain driving accuracy, it is computationally easier to determine the control signals for each motor that make them spin with the same no load speed beforehand. To accomplish this, we can determine a linear relationship between input signal and output motor speed for each of the motors and solve for the input that will produce a given speed. Table 2 lists the slope and y-intercept of these linear relationships.

TABLE 2. DRIVE MOTOR CONTROL EQUATIONS

Motor #	Slope	Intercept
1	77.65	-563.3
2	77.16	-439.6
3	77.30	-477.1

It is possible to use the linear relationships described in Table 2 to calculate the control signals required to make the motors spin at any desired speed within their operating range (~2000 rpm to ~13200 rpm), but it should be noted that the motors are limited to a minimum rpm around 2000 rpm; any control signal that commands a speed lower than this value will not cause any motion in the motor.

The last step necessary to tune the robot before experimentation is to correctly calibrate the gimbal servos so that they can accurately position the gimbal and drive wheels. This is a simple process that begins with zeroing the gimbals by eye. Once this is done, the drive motors are set to spin at a low speed (about 2500 rpm in this case) and the resulting robot movement is observed. Because the drive axles will not be perfectly orthogonal to the ground plane, each wheel will generate a small thrust vector. It is possible to observe the robot motion and adjust the gimbal angles until the wheels no longer roll on the ground but instead spin in place. Iterating through this process a few times allows the gimbals to be zeroed fairly accurately. For the purposes of this experiment, the gimbals were considered to be properly zeroed if the robot did not move more than 1 inch over the course of 30 seconds as the drive motors spun.

4.3 Experimental Results

In this experiment, the desired trajectory of the robot was smooth motion in a 1 meter square at 1 m/sec. This shape was chosen because it allowed for robot motion in all directions, and was small enough to be captured on camera easily. It also allowed for analysis of the robot's open loop performance in a straight line and around sharp corners. The corresponding gimbal angles were calculated using the inverse kinematic equations described above. An example run of this trajectory is shown in Figure 13, below.

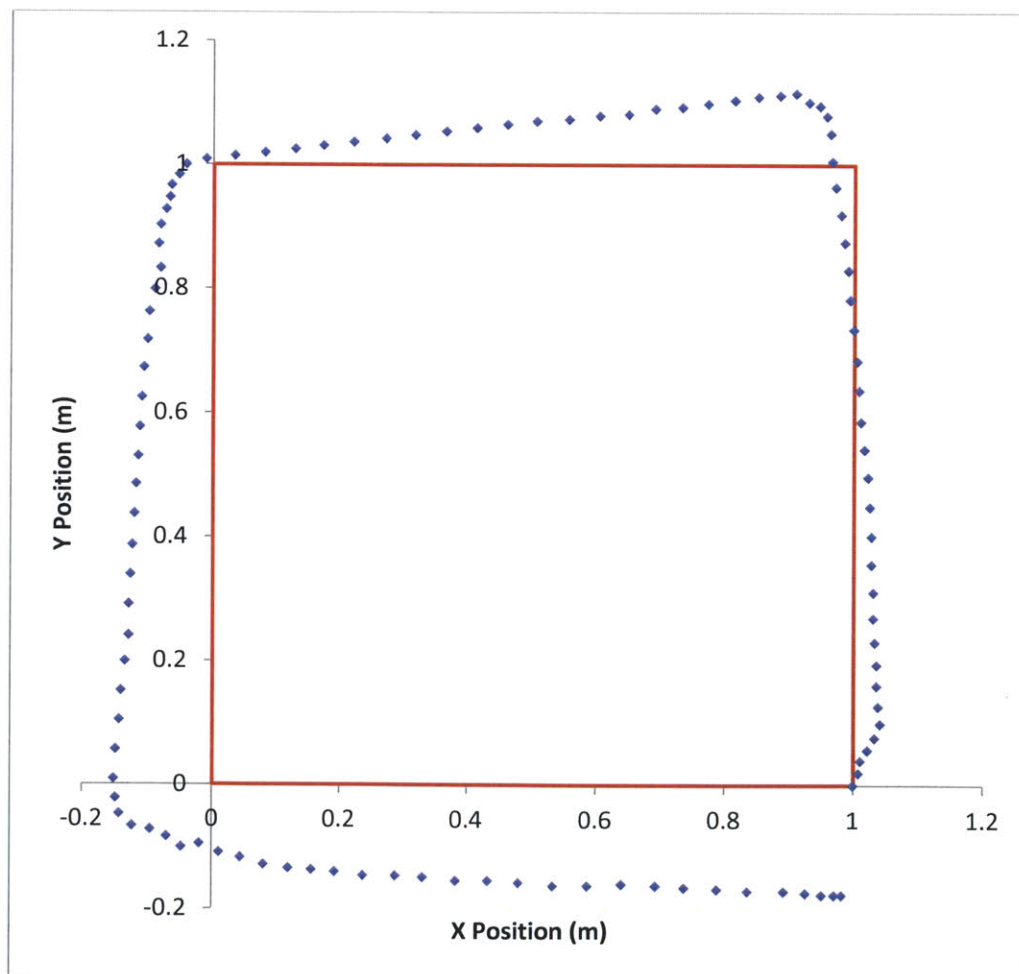


FIGURE 13. POSITION DATA FOR ROBOT TRACKING A 1 METER SQUARE AT 1 M/S

In Figure 13, the blue dots represent the position of the robot's center point as it moved around the square. Shown in red is the reference trajectory. This position information was collected using a small camera mounted on the ceiling and centered above the desired square trajectory. The robot's motion was recorded using this camera, and the resulting film was analyzed using ImageJ software. The square route was marked on the floor with thin strips of masking tape, both to allow the researcher to align the robot for the test and to provide a scale reference for the image analysis. The motion was filmed at 24 frames per second, which implies a time step of $1/24$ seconds (~ 0.0417 sec) between each data point. This time step allowed the approximate speed of the robot to be extrapolated. Figure 14 shows the speed data for the trial run shown above.

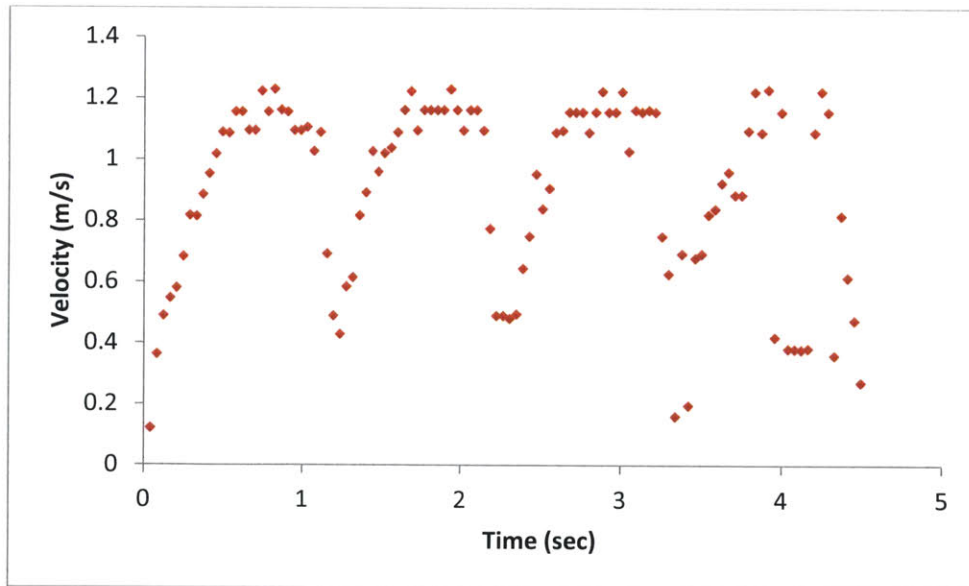


FIGURE 14. ROBOT SPEED DURING SQUARE TRAJECTORY TRACKING TEST

4.4 Analysis of Experimental Results

Referring to Figure 13, it can be seen that the overall path tracking performance by the open loop controller was fairly successful. With a maximum error of only about 16% near the end of the path, it would appear that the kinematic equations derived earlier represent the system accurately.

Most importantly, it can be seen that the robot was able to travel in nearly straight lines around all sides of the square, even if the path of travel did not perfectly match the desired direction. Also important to note was that the observed orientation of the robot with respect to the global reference frame did not change during the straight segments of the square trajectory. This suggests that the kinematic equations derived in Chapter 3 are valid, and the discrepancies between the desired trajectory and the resulting motion of the robot are likely due to outside factors.

To explore some of these discrepancies, first observe the corners of the path taken by the robot. Notice that at each corner the robot decelerates slightly in its initial direction of travel and then reaccelerates in the new direction of travel, causing the path taken to round itself over. This was not a desired effect, instead, it is believed that low friction between the drive wheels and the ground caused significant slipping at these points of high acceleration. Testing was performed on a hardwood floor, where the 3D printed wheels (made of ABS plastic) did not get much traction.

This slipping is also likely the cause of some of the heading errors as well. During the first and second turns especially, the robot did not accurately change its direction of

travel (over-turning on the first turn and under-turning on the second). Calibration and initial testing of the gimbal servos suggests that this was not a gimbal angle error; the internal PID controllers in each Dynamixel servo would have adjusted for the shear forces and torques in the gimbal, maintaining the correct wheel tilt vector. It is more likely that the robot slipping at the corner threw off its orientation, causing the robot's final trajectory to diverge from the desired path.

Finally, errors in the driving velocity contributed to the tracking errors in the robot. As shown in the graph in Figure 14, the robot travelled faster than the intended 1 m/s on the straight segments. This obviously cannot be attributed to slippage in the wheels. Instead the nature of the drive wheel's geometry, as a result of their method of manufacture, is likely to blame. Because they were 3D printed, the hemispherical surface of the wheel was not perfectly smooth. Steps in the wheel surface prevented the desired effective radius from being achieved because the wheel would rest on the edge of a printing layer instead of the desired contact point on the wheel. Thinner 3D printing layers would help reduce this effect and could help to allow for more accurate trajectory tracking.

5. Summary

5.1 Conclusion

In this paper, the design of a triple singularity drive is documented. This concept takes the idea of a singularity drive one step further by increasing the number of singularity drive modules to three, allowing for a increased stability, power, and trajectory tracking accuracy.

The development of this triple singularity drive platform began with the mechanical design. A suitable robot architecture was created using modular components, allowing for quick design changes and repair work. An interlocking acrylic frame provided the support for drive modules and electronics, while advanced Dynamixel servo motors enabled very precise control over the drive angles. An Arduino Mega microcontroller provided accurate control over the operating parameters and a serial interface with a personal computer. Finally, inexpensive yet powerful brushless motors were chosen to provide the thrust forces required by the robot.

An inverse kinematic model of the robot was derived by breaking up the desired trajectory into rotational and translational components. Wheel velocity vectors that matched these components were calculated for each wheel, and recombined by superposition. Corresponding gimbal angles that would produce the correct wheel velocity vectors were calculated using a pair of nonlinear equations. From this model, a forward kinematics model was derived, by taking the pseudo-inverting the inverse kinematics with

a best fit model. This model can solve for the robot's global velocity that is most consistent with the gimbal angle measurements of the overdetermined system.

Validation of this kinematic model was performed with a trajectory tracking test. The robot was given a 1m square path to follow at a given speed, and its resulting motion was captured using an overhead camera. The robot's position over time was analyzed from this camera's feed, and the velocity information was extracted and compared to the desired trajectory. It was found that even without closed loop control, the robot could accurately follow a given trajectory with a maximum of 16% error. Through analysis of the position and velocity information, it was determined low friction between the drive wheels and the ground likely caused most of the path-following error.

5.2 Future Work

This work has a lot of potential to be expanded upon. Most pressing is additional testing with higher friction wheels. This would decrease the amount of slipping that the robot experienced and greatly improve its ability to follow a given trajectory. Similarly, the development of a dynamical model of the robot would allow for closed loop controllers to be implemented, which could improve the tracking of the robot regardless of traction.

Additional improvements can also be made to the mechanical design of the robot. Most important is the design and manufacture of the hemispherical drive wheels. If they were machined on a lathe or CNC mill, the negative effects of the printing layers could be removed, allowing for more accurate control over the effective radius of the wheel in contact with the ground.

6. Bibliography

- [1] Borium, Curt. *Design and Implementation of Novel Hemispherical Omnidirectional Gimbaled Wheel (HOG Wheel) for Mobile Robotics*. Bradley University, 2012.
- [2] Kelly, Alonzo. "A Vector Algebra Formulation of Kinematics of Wheeled Mobile Robots." Thesis. The Robotics Institute of Carnegie Mellon University, 2010. Web.
- [3] Rodić, Aleksandar D. "Modeling and Assessing of Omnidirectional Robots with Three and Four Wheels." *Contemporary Robotics, Challenges and Solutions*. Vukovar: In-Teh, 2009. N. pag. Print.
- [4] West, A. M., and Harry Asada. "Design of Ball Wheel Mechanisms for Omnidirectional Vehicles With Full Mobility and Invariant Kinematics." *ASME Journal of Mechanical Design* 119.2 (1997): 153-61. Web.
- [5] West, Matthew T. *The Design and Control of a Singularity Drive System for an Omnidirectional Vehicle*. Thesis. Bradley University, 2012. Ann Arbor, MI: ProQuest LLC., 2012. Print.